Original Research Article

Targeting PD-1: A Computational Approach to Discover Small Molecule Inhibitors for Cancer Treatment

Abstract

Globally, cancer is a major burden of disease threatening human health. To date, immune checkpoint inhibitors, which are monoclonal antibodies used as monotherapy or in combination, have revealed remarkable clinical success in a wide range of solid tumors and hematologic malignancies. Given the limitations of antibody therapies, orally bioavailable small-molecule inhibitors present a viable alternative.

The discovery of new therapeutic drugs is complex, costly, and time-consuming. Leveraging a combination of computational methods can significantly accelerate the drug discovery process, enabling the identification of promising drug candidates from the large compound libraries. In the Silico Computational study, 30 hit compounds were initially retrieved by pharmacophore-based virtual screening. Thereafter, 5 compounds with lowest Gibb's free energy (ΔG) values, namely ZINC85867378, ZINC16267039, ZINC64219346, ZINC68604154 and ZINC20576138, have been chosen for further evaluation. This study establishes the workflow combining pharmacophore virtual screening, molecular docking, and absorption, distribution, metabolism, excretion - toxicity (ADMET) prediction to identify possible small molecules that can interact with PD-1. The identified compounds might serve as starting points to design potential safe and efficacious molecules in cancer Immunotherapy. Further evaluation is necessary to optimize drug properties.

Keywords: PD-1, small molecule inhibitors, cancer immunotherapy, immune checkpoints, computer aided drug design

1. Introduction

Cancer is a major burden of disease threatening human health based on its high rates of morbidity and mortality [1]. Globally, the number of new cases and deaths due to cancer were estimated to be 19.3 million and almost 10 million, respectively, in 2020 [2]. There are an estimated 2.3 million new cases of breast cancer (12.7%), followed by lung (12.4%), colorectal (10.0%), prostate (7.3%), and stomach (5.6%) [2].

Cancer occurs when normal cells undergo a multistage transformation into tumor cells. It has been considered that altered metabolism in tumor cells is to facilitate their rapid duplication and growth [3]. Sustaining proliferative signaling, evading growth suppressors, resisting cell death, enabling replicative immortality, and activating invasion and metastasis are essential hallmarks of cancer, among which, immune escape is a particularly critical phase of carcinogenesis [4]. The malignant cells escaping from immune surveillance can gradually break the balance between the transformed cells and immunity by sculpting the tumor immune microenvironment (TIME) [5]. Consequently, the immune system loses the potential to recognize and eradicate these kinds of malignant cells and let them form clinically visible cancers.

In previous decades, the most common types of cancer treatments were surgery, radiotherapy, and chemotherapy[6]. Recent advances in immunotherapy, a type of cancer treatment harnessing the immune system to fight cancer, established itself as one of the pillars of cancer treatment improving the prognosis of patients with different hematological and solid malignancies. Immune checkpoints, which are a plethora of inhibitory mechanisms hardwired into the immune system, are important for modulating the duration and amplitude of physiological immune responses in tissues in order to limit collateral tissue damage [7]. To date, immune checkpoint inhibitors (ICIs) are monoclonal antibodies that block immune checkpoints to augment T-cell–mediated tumor destruction [8]. ICIs in current clinical settings target programmed death-1 (PD-1), programmed death-ligand 1 (PD-L1), or cytotoxic T lymphocyte antigen 4 (CTLA-4) are regarded as breakthroughs in cancer immunotherapy [9-11].

PD-1/PD-L1 pathway regulates the induction and maintenance of immune tolerance in the tumor microenvironment. Crystal Structure of the PD-1/PD-L1 Complex is displayed in Fig. 1 [12]. PD-1 (or CD279), a 50–55 kilodalton Type 1 transmembrane glycoprotein, is a member of the CD28 family of T-cell co-stimulatory receptors that include immunoglobulin super family members CD28, CTLA-4, inducible co-stimulator (ICOS), and B and T lymphocyte attenuator (BTLA) [13]. This factor was named programmed cell death protein 1, because its expression was shown to be enhanced by apoptotic stimuli

in two different cell lines (LyD9, a murine hematopoietic progenitor cell line and 2B4.11, a murine T-cell hybridoma), and it participates in apoptosis [14]. PD-1 is mainly expressed on activated T cells, B cells, monocytes, dendritic cells (DCs), regulatory T cells (Tregs), and natural killer T cells (NKT) [15].

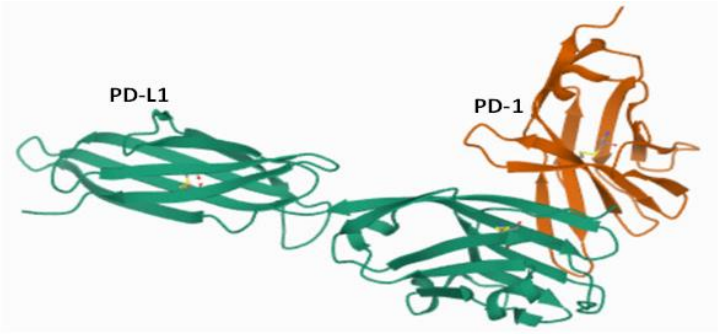

Fig.1 Crystal Structure of the PD-1/PD-L1 Complex (PDB ID: 3BIK) [12]

Two ligands specific for PD-1 have been identified: PD-L1 (B7-H1 or CD274) and PD-L2 (B7-DC or CD273). In tumor cells, both in solid tumors and hemangiomas, PD-L1 is generally upregulated. PD-L1 is also expressed on T cells, B cells, macrophages, dendritic cells (DCs), bone marrow-derived mast cells and some non-immune cells, hence can thus be regarded as the major PD-1 ligand [16, 17]. The expression of PD-L2 is greatly limited to professional antigen presenting cells (APCs) like macrophages and DCs. In both murine and human systems, PD-L1 and PD-L2 have been shown to down-regulate T-cell activation upon binding to PD-1 [18-20]. The absence or inhibition of PD-1 has resulted in the development of various autoimmune phenotypes and autoimmune diseases. [21] The interaction of PD-1 with its ligands PD-L1 and/or PD-L2 are responsible for T cell activation, proliferation, and cytotoxic secretion in cancer to degenerating anti-tumor immune responses [22]. (Fig.2) Accumulating evidence indicates that the inhibition of PD-1 binding to its ligands promotes an effective immune response against cancer cells.

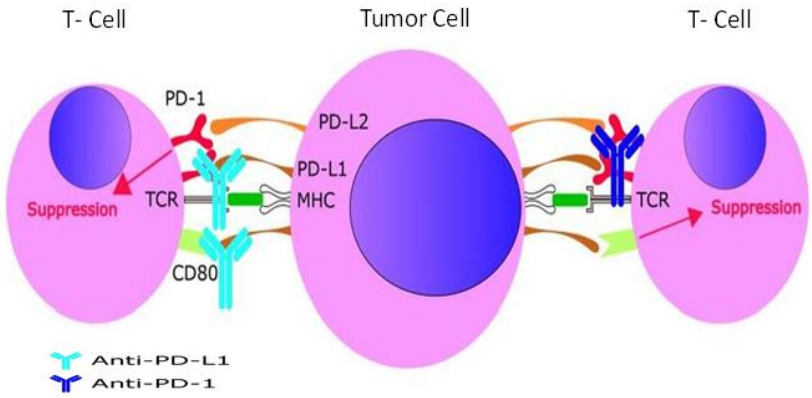

Fig. 2. Concept of therapeutic interruption of the PD1-PD-L1 axis to disrupt the tumor cell induced downregulation of the T cell mediated cytotoxic immune response [23].

Currently, more than 3000 clinical trials (phase I–III) of anti-PD-1/anti-PD-L1 antibodies are ongoing. Either alone or in combination with chemotherapy and/or immunotherapy for patients with hematologic malignancies and solid tumor including NSCLC, esophageal cancer, ovarian cancer, renal cell carcinoma, and mantle cell lymphoma etc [24]. The U.S. Food and Drug Administration (FDA) and the European Medicines Agency (EMA) have approved several anti–PD-1 (nivolumab, pembrolizumab, and cemiplimab)/PD-L1 (atezolizumab, avelumab, and durvalumab) immune checkpoint inhibitors covering various cancer indications as monotherapy or in combination with other drugs, have revealed remarkable clinical success in in a wide range of solid tumors and hematologic malignancies [25]. In addition, toripalimab and camrelizumab were approved by National Medical Products Administration (NMPA) for marketing.

There are some limitations associated with the antibody-based therapies, such as immunogenicity, immune-related adverse events (irAEs), limited modes of administration (intravenous and subcutaneous), low penetration into tissues and high cost. Alternatively, small molecule inhibitors may have advantages such as favorable tumor penetration, fewer side effects, easier self-administered, less expensive than mAbs etc. Therefore, developing orally bioavailable small molecular inhibitors (usually below 0.5 kDa) to block the PD-1/PD-L1 pathway (and other immune checkpoints) has emerged as an important area of drug discovery research [26, 27].

During the past several years, many companies, such as Aurigene and Curis, Bristol Myers Squibb (BMS), MaxiNovel Pharmaceuticals and Incyte Corporation etc, have discovered a series of peptides and small molecules for the inhibition of the PD-1/PD-L1 axis. Currently, most small molecule inhibitors targeting PD-1/PD-L1 signaling pathway are still in the early development stage [24]. To our knowledge, CA-170 (discovered by Aurigene and Curis) is the first orally peptidomimetic PD-L1 inhibitor entering into clinical trials. CA-170 was screened from B7 immunoglobulin superfamily members in a checkpoint protein interaction surface simulant library, which could selectively target PD-L1 and VISTA (V-domain Ig suppressor of T cell activation) pathways. VISTA (approximately 50kDa) is part of the B7 family of immune checkpoint proteins, and shares 22% of the sequence with PD-L1[28]. In multiple preclinical models, CA-170 has shown anti-tumor activity[29]. However, some evidences suggest CA-170 does not bind to PD-L1 and cannot disrupt PD-1/PD-L1 complex[30]. In the phase II study, CA-170 showed antitumor responses in two patients with Hodgkin's lymphoma, and the clinical benefit rate is 68.18%. CA-170 was permanently discontinued without any sequalae, suggesting that shorter half-life (6-8 hours)

of CA-170 may provide an advantage over longer lasting antibodies, from safety perspective [31]. The first non-peptide inhibitor targeting PD-1/PD-L1 interaction was discovered by BMS and was based on (2-methyl-3-biphenylyl) methanol scaffold [32]. Using ^{15}N-labeled PD-L1 and PD-1 and NMR-based antagonist induced dissociation assay (AIDA) assay, Tad A. Holak's group showed that BMS's compounds bind to PD-L1 and dissociate the human PD-1/PD-L1 complex [33]. MaxiNovel Pharmaceuticals discovered a series of PD-1/PD-L1 inhibition molecules based on BMS's methyl biphenyl scaffold with the replacement of benzyl ether moiety using ethenyl or ethynyl linkage [34]. Incyte Corporation has also reported several patents based on BMS's biaryl moiety and launched a phase I clinical study using INCB86550 for treatment of solid tumors[34].

The discovery of new therapeutic drugs is complex, costly, and time-consuming. Nowadays, computer aided drug design (CADD) approaches become the most effective methods to discover and develop drugs. In CADD workflows, pharmacophore models can identify active molecules against specific targets. Binding affinity of a large-scale compounds can also be evaluated easily by molecular docking process [35, 36]. To find new anticancer agents, structure-based pharmacophore models based on promising cancer therapy targets (such as glycogen synthase kinase-3, protein kinase B-beta, matrix metalloproteinase-2, and histone deacetylase-6) have been used [37, 38]. Pharmacokinetic properties (absorption, distribution, metabolism, excretion) and toxicity, referred to as ADME-tox, are also of vital importance if a compound is to be clinically useful. ADME-tox profile of drug-like compounds can be predict by using CADD process as well [39].

The aim of this project is to mainly focus on CADD process to predict the possible small molecules that can interact with PD-1, and further serve as starting points to design potential safe and efficacious compounds in cancer treatment.

2 Materials and Methods

2.1 Research workflow

In the current study, a computational approach was used to identify several small molecules interact with the crystal structure of PD-1. No statements of approval or informed consent were required for our study as we obtained data from an open access database. A research workflow is presented in Fig. 3.

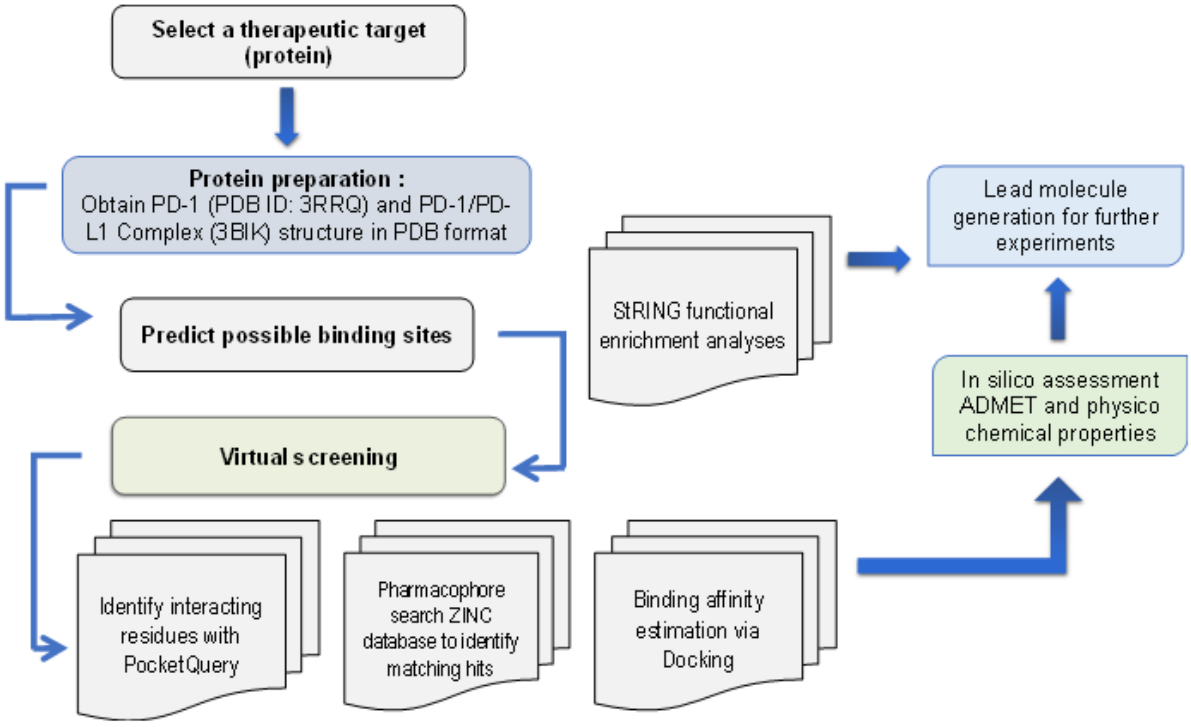

Fig. 3: Research Workflow of predicting small molecules interact with the crystal structure of PD-1 as potential therapeutics for cancer immunotherapy

2.2 Protein preparation

Crystal structures of human PD-1 (PDB ID: 3RRQ) and the PD-1/PD-L1 Complex (3BIK) were obtained in PDB format from the RCSB (Research Collaboratory for Structural Bioinformatics) protein data bank (www.rcsb.org) [40]. The stereochemistry of the protein structure was analyzed by the PROCHECK tool (http://services.mbi.ucla.edu/PROCHECK/) for assessing the quality on the basis of Ramachandran Plot [41].

2.3 Ligand binding site identification

DoGSiteScorer (freely available on the ProteinsPlus server, https://proteins.plus/), FTsite (https://ftsite.bu.edu/) and PrankWeb (https://prankweb.cz/) servers have been used for the identification of ligand binding sites on the protein structure.

2.3.1 DoGSiteScorer

DoGSiteScorer[42] is a grid-based approach which uses a difference of gaussian filter to detect potential binding pockets. A druggability score between 0 and 1 is reported. A higher score indicates that a pocket

is more likely to be druggable. PDB code has been entered into the search box on the ProteinsPlus server and then press the "Go" button. Next, choose DoGSiteScorer and press the "Calculate" button for running DoGSiteScorer with default settings for the results.

2.3.2 FTSite

FTSite is an energy-based approach[43] by using a solvent mapping algorithm which places each of different small molecular probes on a dense grid around the protein and finds favorable positions using empirical free energy function. The individual probes are clustered, and the clusters are ranked based on the average free energy. PDB code has been entered into the search box on the FTsite server. Then input the job name and email address to receive notification upon the job is finished. Next, press the "Find My Binding Site" button for running FTsite with default settings for the results.

2.3.3 PrankWeb

PrankWeb is a recently developed online web server that provides an interface for the P2Rank method[44]. P2Rank is a template-free machine-learning algorithm that does not rely on the structural information available for other protein-ligand complexes and thus enables the discovery of truly novel binding pockets[45]. PDB code has been entered into the search box on the PrankWeb server and then press the "Submit" button for running PrankWeb with default settings for the results.

2.4 Pharmacophore query construction

The pharmacophore query for the PD-1/PD-L1 complex (PDB ID: 3BIK) interfaces was built using the PocketQuery feature generation protein-protein interaction (PPI) target-based capability. PocketQuery (http://pocketquery.csb.pitt.edu/) is an online platform to identify hotspot amino acids and drug binding sites[40]. PocketQuery predicts the druggability of a residue, maximum cluster distance (Dist), the change of solvent accessible surface (SASA) area upon complexation (ΔSASA), percentage of the total possible SASA(ΔSASA%), estimation of the change of free energy of an alanine mutation (Rosetta Energy (ΔΔG), the change of free energy of a residue upon complexation (FastContact Energy (ΔG)), a sequence conservation score, and an evolutionary rate of the residue[46]. PDB code has been entered into the search box on the PocketQuery server and then press the "Search" button for running PocketQuery with default settings for the results.

2.5 Pharmacophore-based virtual screening

The 6 highest ranked clusters obtained from PocketQuery were used as a query for pharmacophore-based virtual screening through ZincPharmer, which is an online platform (http://zincpharmer.csb.pitt.edu) for screening the commercially available compounds in the ZINC database. It utilizes the searching algorithm of Pharmer.[40] ZINCPharmer offers several options for designing and modifying pharmacophore hypotheses straight from molecular organization of the ligand and protein.

2.6 Docking-based virtual screening

Molecular docking was carried out in the study to evaluate the binding ability of the hit compounds to the target PD-1 protein. Selected hit compounds obtained by pharmacophore screening were subject to molecular docking, which was performed using SwissDock under the accurate mode (http://www.swissdock.ch). SwissDock is a web server dedicated to the docking of small molecules on target proteins, based on the based on the dihedral space sampling (DSS) in EADock[47]. Docking interactions were revealed by full fitness and Gibbs free energy prediction.

Crystal structure of PD-1 (PID ID: 3RRQ) obtaining from the protein data bank website has been upload to SwissDock as "target selection". Zinc ID identified by PocketQuery has been entered as "ligand selection". If zinc ID has not been found by SwissDock, then chemical structures of the ligand compounds were obtained from cheminfo.org web-based platform by converting smiles format to mol2 standard file. Next, upload the converted mol2 file to SwissDock as "ligand selection". Input the job name and email address to receive notification upon the job is finished. Then press the "Start Docking" button to perform molecular docking for the results. Furthermore, docking interactions of the selected molecules with CTLA-4 (PDBID: 3OSK) were also explored.

2.7 Drug likeness property and ADME-tox prediction

The SWISSADME server was used to analyze the Drug-like properties of the selected molecules (http://www.swissadme.ch/)[48]. After that, the ADME-tox evaluation for each of the molecules was conducted by the online based server, ADMETlab (https://admetmesh.scbdd.com/). It predicted various pharmacokinetic and toxicity profiles[49]. For the convenience interpolation, the numeric and categorical values of the results generated by the ADMETlab server were converted into qualitative values according to the documentation described online. Smiles format of each selected molecule has been entered as input to SWISSADME or ADMETlab. Then press the "submit" button to perform analysis with default settings

for the results. Water-soluble, satisfy Lipinski rule, relatively good bioavailability and safety profiles (i.e., risk for liver toxicity) were considered as molecules selection criteria.

2.8 Protein-protein interaction map

Protein-protein interaction map for PD-1 and CTLA-4 was constructed using search tool for the retrieval of interacting genes/proteins (STRING v11)[50]. Active interaction sources were restricted to "Textmining", "Experiments" and "Databases". Only interactions with confidence score over 0.9 were mapped to the network. The nodes in the PPI network represented the proteins, and the edges between the nodes represented the interactions between them. The node with a high degree was deemed with an essential biological function.

3 Results

3.1 Structural assessment

The protein structures of PD-1 and PD-1/PD-L1 complex were validated using PROCHECK tool. The Ramachandran plot interprets those residues under most favored regions are 92.3% and 90.0% for PD-1 and PD-1/PD-L1 complex, respectively (Fig. 4).

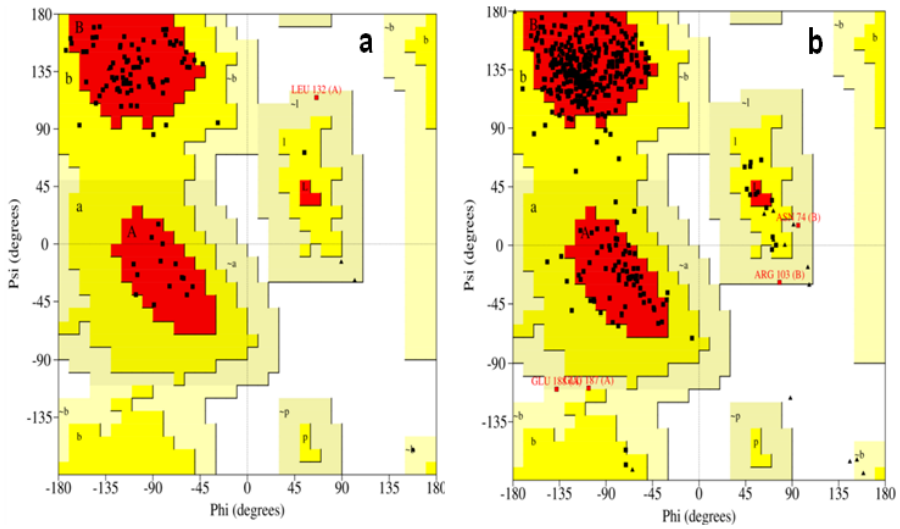

Fig. 4 Ramachandran plot of PD-1 (a) and PD-1/PD-L1 complex (b)

3.1 Ligand binding site identification

Identifying protein–ligand binding sites, or more broadly, any favorable regions for interaction with small molecules, play a vital role to provide biological insights for protein function.

3.1.1 DoGSiteScorer

The investigation results on the ProteinsPlus DoGSiteScorer server show that there are four prospective binding sites (Table 1 and Fig. 5). Pockets with a higher druggability score are considered more likely druggable. Target druggability encompasses not only the ability of protein binding sites to be complementary with small molecules in terms of physicochemical properties (like size, shape, electrostatics and hydrophobicity) – in order to successfully bind them with high affinity – but also the ability to bind small molecules holding certain physicochemical properties that place them in the so-called "drug-like" property space, implying that a binding site is suitable for interactions with molecules that may be optimized into a therapeutic drug candidate. A druggable pocket generally is characterized by large pocket volume, high depth as well a high apolar amino acid ratio, meaning that this pocket is considered druggable. The largest pocket (P_0), represented in orange, has a depth value of 13.75 Å and a ratio of apolar amino acids of 0.47. The pocket (P_1) represented in orange, has a depth value of 116.23 Å and a ratio of apolar amino acids of 0.47. The pocket (P_2) represented in green, has a depth value of 9.38 Å and a ratio of apolar amino acids of 0.64. The pocket (P_3) represented in red, has a depth value of 9.45 Å and a ratio of apolar amino acids of 0.45.

Table 1. The four binding pockets for PD-1 (PDB ID: 3RRQ) predicted by DoGSiteScorer.

Pocket	Volume (Å^3)	Surface (Å^2)	Drug Score
P_0 (a)	238.78	593.75	0.55
P_1 (b)	209.79	319.8	0.62
P_2 (c)	153.92	326.88	0.33
P_3 (d)	127.74	329.38	0.29

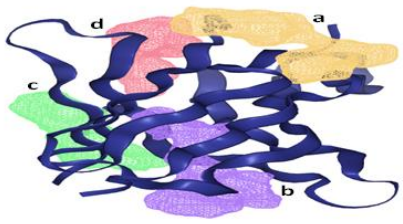

Fig. 5 Predicted binding pockets with highlighted in orange, purple, green and red.

3.1.2 FTSite

The investigation results on the FTSite server show that there are three prospective binding sites on the PD-1 protein (PDB_ID: 3RRQ). The detected sites have the following residues: site a (pink)— Ile134, Glu136, Leu122, Met70, Tyr68, Lys78; site b (green)_— Asp 77, Thr76, Gln75, Arg69; site c (purple)— Leu79, Phe95, Cys93, Ala80, Arg96, Ala81, Val97, Thr98, Glu84, Phe82, Pro83, Gln99 (Fig. 6).

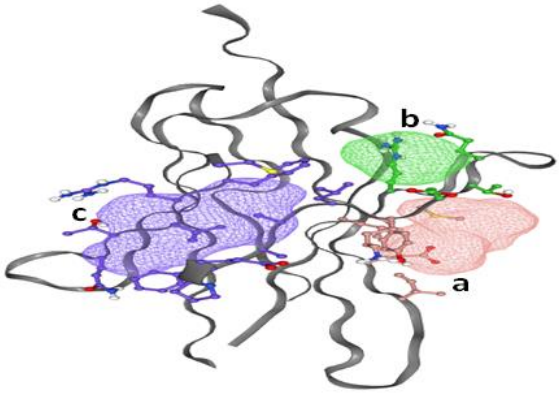

Fig. 6. Predicted three binding sites with highlighted in red, green and purple using FTSite for PD-1 (PDB ID: 3RRQ).

3.1.3 PrankWeb

The investigation results on the PrankWeb server show that there is one prospective binding site (Fig. 7). The binding site has pocket score 1.24. The detected site has the following residues: site (blue) — Arg69, Gln75, Asp77, Leu79, Phe95, Asn116, Asp117.

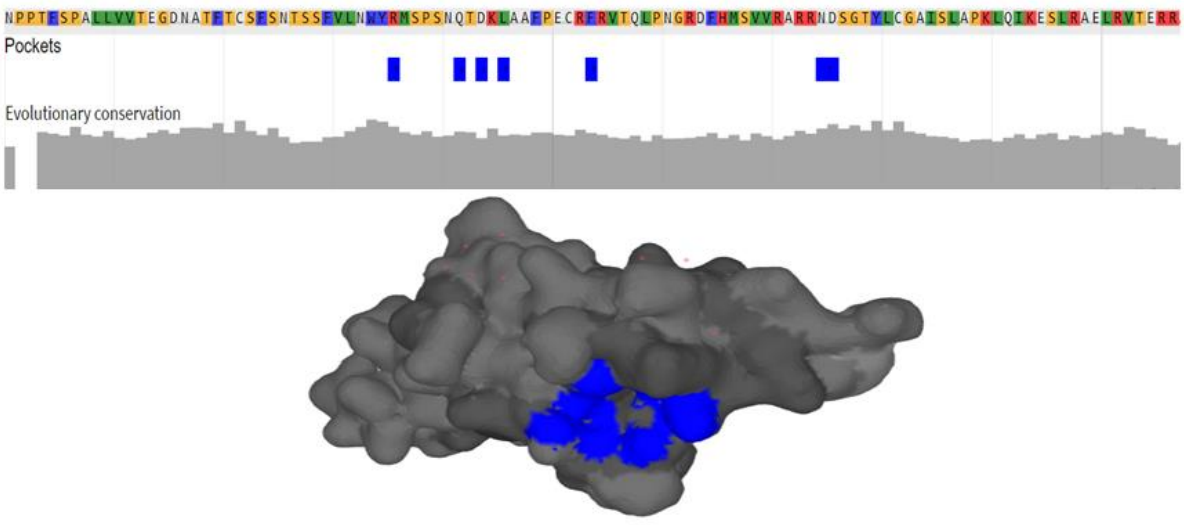

Fig. 7: Predicted binding sites with highlighted in blue using Prank Web for PD-1 (PDB ID: 3RRQ).

3.2 Pharmacophore query construction

Top rank 6 clusters selected based on the "druggability" score were presented in Table 2. Clusters are ranked according to a 'druggability' score where high scoring clusters likely delineate potential binding sites on the PD-1/PD-L1 complex surface. Cluster 1 (TYR123, ARG125) has a highest score of 0.81099. The PocketQuery pharmacophore search results for targeting the PD-1/PD-L1 complex were visually evaluated as well (Fig. 8).

Table 2. Summary of top rank 6 clusters obtained from PocketQuery for targeting the PD-1/PD-L1 complex.

Cluster	Ch	Residues	Dist	ΔG^{FC}	$\Delta\Delta G^{R}$	ΔSASA	ΔSASA%	Score
1	A	TYR123; ARG125	6.9848	-5,765	1.1088	111.72	59.45	0.81099
2	A	MET115; TYR123; ARG125	11.866	-4.5333	1.03887	91.5967	50.5667	0.773548
3	A	MET115; ARG125	11.866	-6.09	0.7063	78.935	42.9	0.76033
4	A	MET115; AYR123; LYS124; ARG125	11.866	-3.64	0.838675	84.435	47.55	0.744317
5	A	ARG113; MET115; TYR123; ARG125	11.866	-4.97	0.84275	74.985	41.05	0.740154
6	A	ARG113; MET115; TYR123; LYS124; ARG125	11.866	-4.168	0.72182	72.578	40.54	0.722176

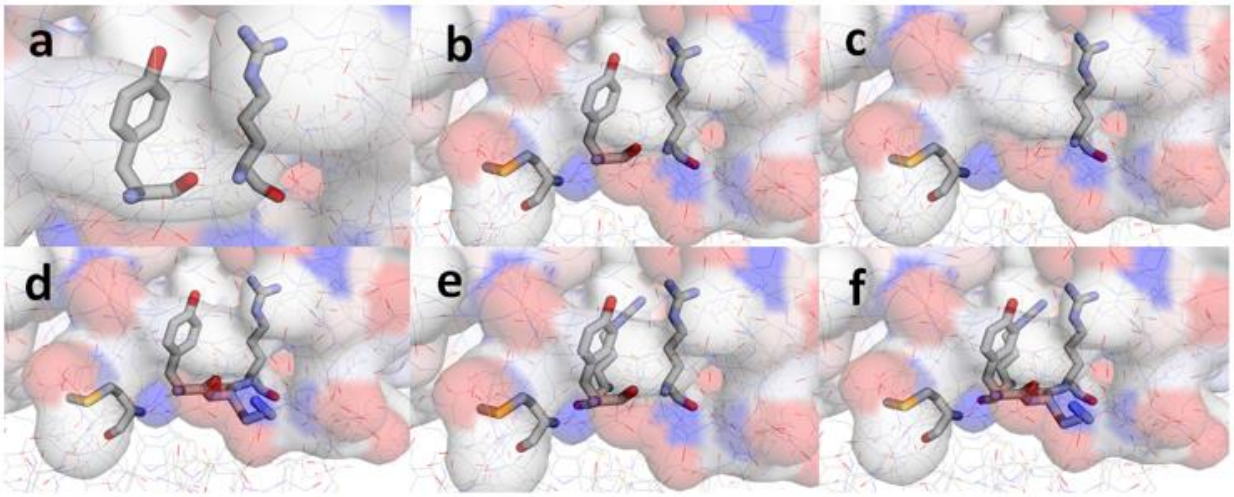

Fig. 8. Molecular viewer of top rank 6 clusters and their properties obtained from PocketQuery for targeting the PD-1/PD-L1 complex

3.3 Pharmacophore-based virtual screening

Results of various hit compounds identified by virtual screening from ZINCPharmer with pharmacophore queries have been presented at Table 3 and Fig. 9. A total 30 compounds were retrieved for molecular docking after removing duplicate compounds. If duplicate compounds were displayed, hit molecules having lower Root Mean Square Deviation (RMSD) values from the binding sites of pharmacophore were chosen. In addition, if more than 100 hits revealed, 10 unique hit molecules having lowest RMSD values were considered.

Table 3. Results of pharmacophore screenings from ZINCPharmer

Cluster	Pharmacophore class	x	y	z	radius	Compound	RMSD	Mass	Rbnds
1	Hydrogen Acceptor	11.85	-8.41	-26.35	0.50	ZINC16267039,	0.409,	461,	13
	Hydrogen Acceptor	16.21	-9.73	-32.11	0.75	ZINC71788370,	0.425,	619,	15
	Positivelon	15.11	-2.11	-30.40	1.00	ZINC71788370,	0.426,	619,	15
	Hydrophobic	9.68	-5.24	-26.78	1.00	ZINC35326858,	0.447,	497,	14
						ZINC85867378,	0.475,	587,	15
						ZINC85867378,	0.506,	587,	15
						ZINC15074281,	0.519,	377,	7
						ZINC58157707,	0.524,	429,	10
						ZINC09805413,	0.544,	434,	7
						ZINC55211811,	0.548,	432,	15
						ZINC73804990,	0.567,	364,	11
						ZINC68604154,	0.567,	373,	8
						ZINC14041891,	0.595,	495,	10
						ZINC24885055,	0.601,	470,	11
						ZINC92061782,	0.604,	371,	8
						ZINC19741916,	0.606,	424,	11
2	Hydrogen Acceptor	16.21	-9.73	-32.11	0.50	ZINC09354187,	0.493,	516,	15
	Positivelon	15.11	-2.11	-30.40	0.75	ZINC36026070,	0.523,	416,	11
	Hydrophobic	9.68	-5.24	-26.78	1.00	ZINC09354187,	0.567,	516,	15
	Hydrophobic	2.87	-9.76	-27.13	1.00				
3	Hydrogen Acceptor	14.16	-8.63	-30.64	0.50	ZINC01081956,	0.502,	475,	10
	Hydrogen Acceptor	16.21	-9.73	-32.11	0.50	ZINC39518974,	0.510,	435,	12
	Positivelon	15.11	-2.11	-30.40	0.75	ZINC09350963,	0.537,	531,	15
	Hydrophobic	2.87	-9.76	-27.13	1.00	ZINC64219346,	0.539,	519,	15
						ZINC39518974,	0.555,	435,	12
4	Hydrogen Acceptor	16.21	-9.73	-32.11	0.50	ZINC09354187,	0.493,	516,	15
	Positivelon	15.11	-2.11	-30.40	0.75	ZINC36026070,	0.523,	416,	11
	Hydrophobic	9.68	-5.24	-26.78	1.00	ZINC09354187,	0.567,	516,	15
	Hydrophobic	2.87	-9.76	-27.13	1.00				
5	Positivelon	11.70	-2.97	-33.30	0.75	ZINC02101516,	0.183,	469,	10
	Positivelon	15.11	-2.11	-30.40	0.75	ZINC02101503,	0.184,	455,	9
	Hydrophobic	9.68	-5.24	-26.78	1.00	ZINC02101516,	0.185,	469,	10
	Hydrophobic	2.87	-9.76	-27.13	1.00	ZINC02101649,	0.188,	455,	9
						ZINC02101649,	0.194,	455,	9
						ZINC12495898,	0.302,	390,	8
						ZINC12495881,	0.311,	388,	7
						ZINC12495895,	0.335,	417,	10

						ZINC04323062,	0.352,	400,	12
						ZINC20576111,	0.377,	481,	8
						ZINC20576138,	0.377,	502,	7
						ZINC20576116,	0.378,	481,	8
6	Positive ion	11.70	-2.97	-33.30	0.75	ZINC02101516,	0.183,	469,	10
						ZINC02101503,	0.184,	455,	9
	Positivelon	15.11	-2.11	-30.40	0.75	ZINC02101516,	0.185,	469,	10
						ZINC02101649,	0.188,	455,	9
	Hydrophobic	9.68	-5.24	-26.78	1.00	ZINC02101649,	0.194,	455,	9
						ZINC12495898,	0.302,	390,	8
	Hydrophobic	2.87	-9.76	-27.13	1.00	ZINC12495881,	0.311,	388,	7
						ZINC12495895,	0.335,	417,	10
						ZINC04323062,	0.352,	400,	12
						ZINC20576111,	0.377,	481,	8
						ZINC20576138,	0.377,	502,	7
						ZINC20576116,	0.378,	481,	8

ZINC19741916 ZINC73804990 ZINC71788370 ZINC85867378 ZINC58157707

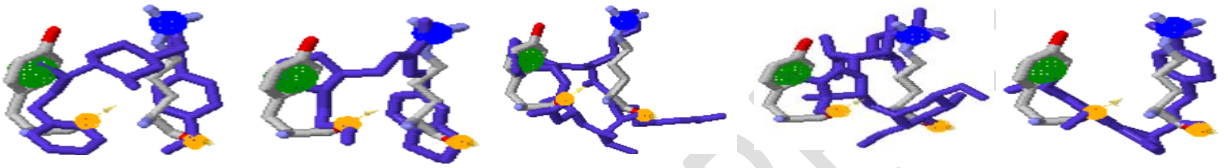

ZINC14041891 ZINC24885055 ZINC35326858 ZINC09805413 ZINC55211811

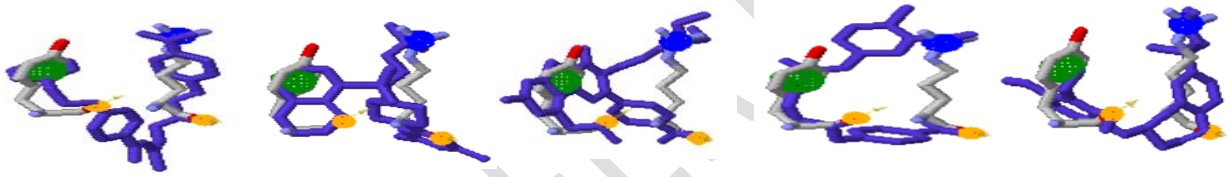

ZINC15074281 ZINC92061782 ZINC16267039 ZINC68604154 ZINC36026070

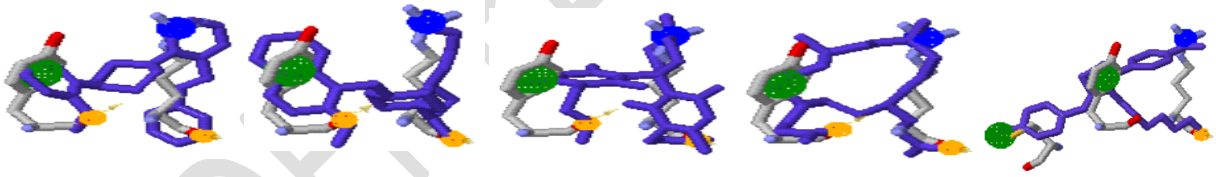

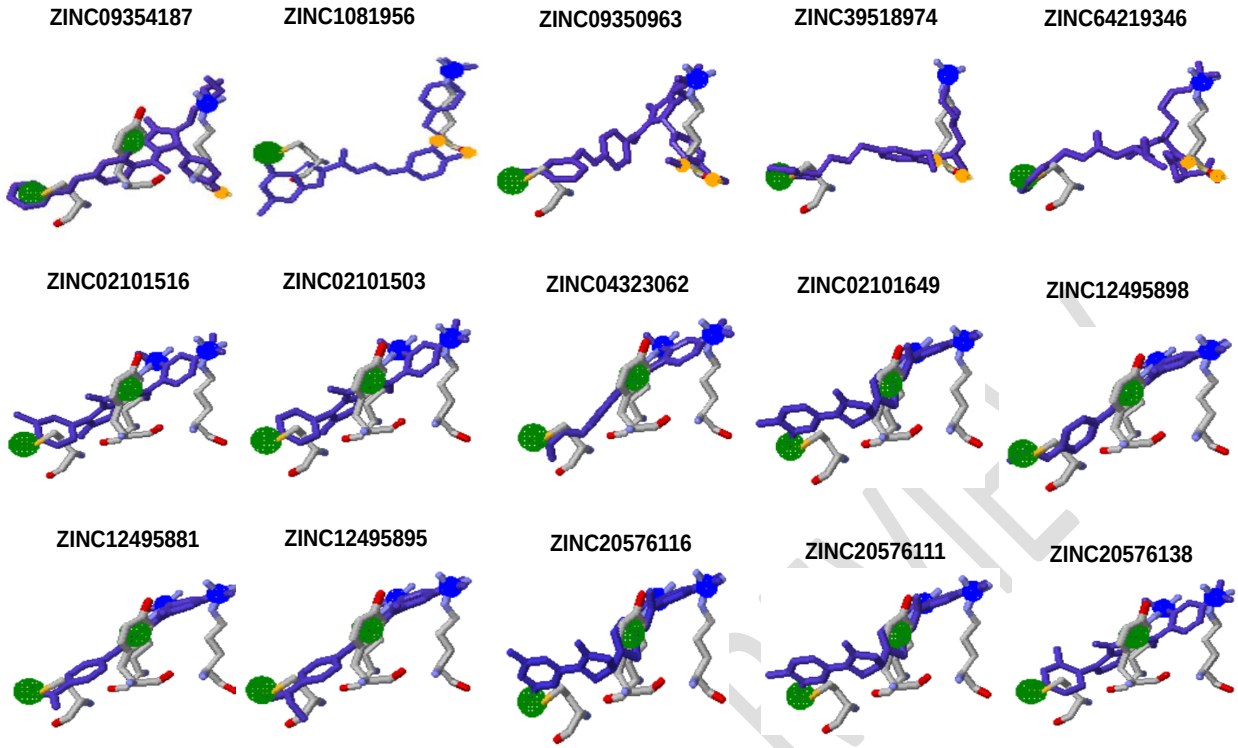

Fig. 9 Results of pharmacophore screenings from ZINCPharmer. Molecules selected for screening based on the pharmacophore features represented as blue sticks, superimposed with the query ligand, showed as grey sticks. Pharmacophore features are shown in spheres. The color classification of the features is hydrogen acceptor (orange), hydrophobic (green) and positive ion (blue).

3.4 Molecular docking

3.4.1 Docking result of selected hit compounds with PD-1 (PID ID: 3RRQ)

The results of Swiss Dock showed full fitness and Gibbs free energy values in kcal/mol are presented in Table 4 & Fig.10. More negative the ΔG value of the binding reaction was considered to have higher the binding affinity. Among the total 30 unique compounds retrieved for molecular docking, ZINC85867378, ZINC16267039, ZINC64219346, ZINC68604154 and ZINC20576138 are the top rank 5 compounds with lowest ΔG values (<-9 kcal/mol), exhibiting possible stronger bindings with PD-1. In addition, no direct correlation has been established between ΔG values from molecular docking and RMSD values from pharmacophore screening (R^2 0.049).

Table 4. SwissDock interaction result of selected hit compounds with PD-1 (PID ID: 3RRQ)

Compound	Full fitness (kcal/mol)	Gibbs free energy Δ(kcal/mol)
ZINC85867378	-829.97	-12.09
ZINC16267039	-790.13	-9.65
ZINC64219346	-861.03	-9.32
ZINC68604154	-814.96	-9.07

ZINC20576138	-686.02	-9.03
ZINC20576116	-684.26	-8.92
ZINC20576111	-681.79	-8.83
ZINC92061782	-699.61	-8.53
ZINC39518974	-636.16	-8.47
ZINC73804990	-791.81	-8.4
ZINC71788370	-838.83	-8.4
ZINC09354187	-682.66	-8.35
ZINC12495881	-695.87	-8.21
ZINC35326858	-699.82	-8.11
ZINC09350963	-641.97	-8.07
ZINC09805413	-678.42	-8.05
ZINC01081956	-602.92	-8.05
ZINC14041891	-643.34	-7.99
ZINC55211811	-618.89	-7.95
ZINC19741916	-667.96	-7.93
ZINC12495898	-700.5	-7.86
ZINC12495895	-708.69	-7.79
ZINC58157707	-694.08	-7.63
ZINC24885055	-772.31	-7.6
ZINC36026070	-712.08	-7.51
ZINC02101503	-659.87	-7.32
ZINC02101516	-661.95	-7.1
ZINC04323062	-647.72	-7.08
ZINC02101649	-656.41	-7.02
ZINC15074281	-615.25	-6.97

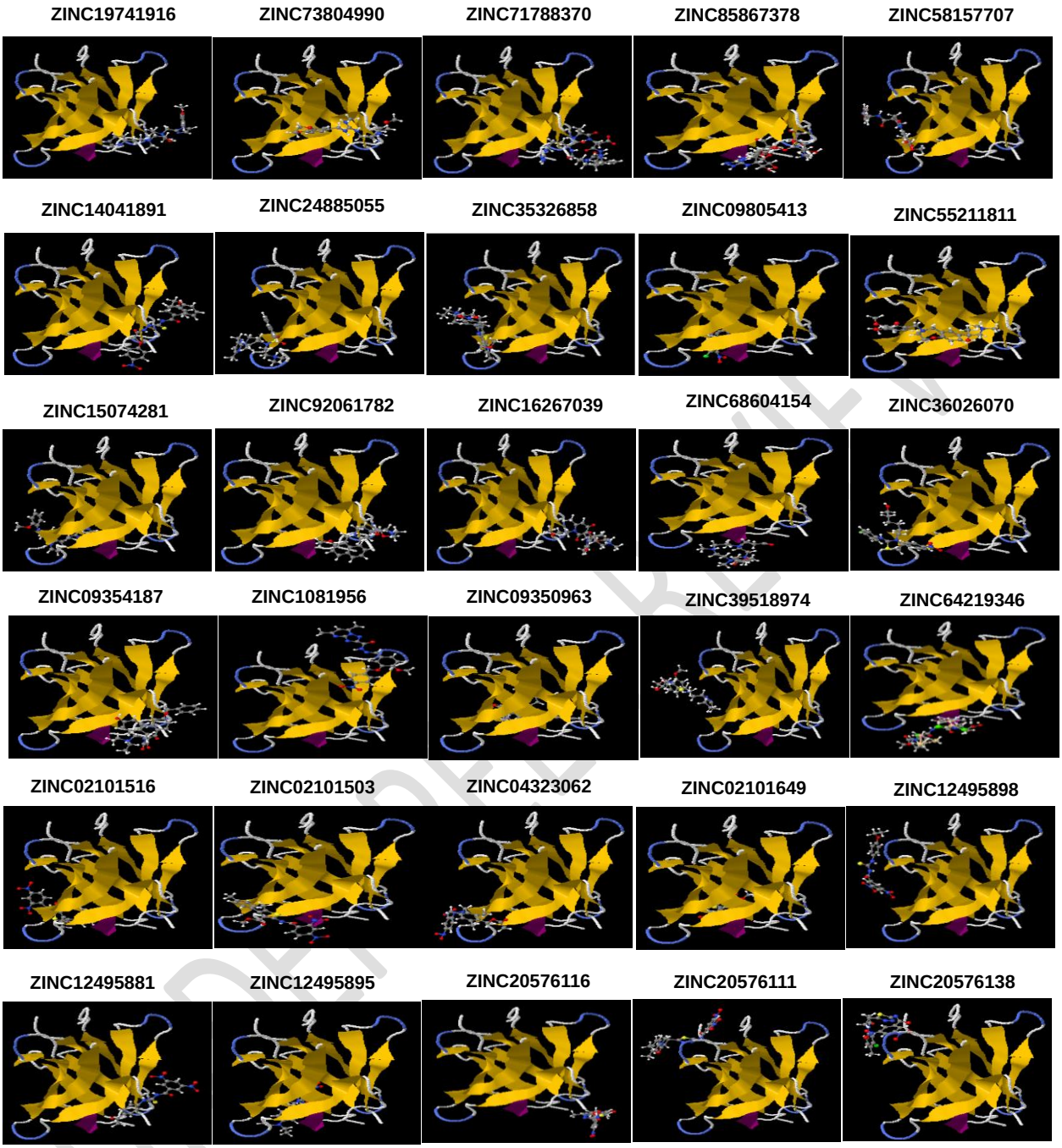

Fig. 10 SwissDock interaction result of selected hit compounds with PD-1 (PDBID:3RRQ)

3.4.2 Docking result of selected hit compounds with CTLA-4 (PDBID: 3OSK)

Five selected molecules (ZINC85867378, ZINC16267039, ZINC64219346, ZINC68604154 and ZINC20576138), which have possible stronger bindings with PD-1 (Gibbs free energy < - 9 kcal/mol), have been chosen for further docking with CTLA-4 protein. (Fig. 11) Among them, ZINC85867378,

ZINC16267039, ZINC64219346, ZINC68604154 and ZINC20576138 have binding affinity −7.760 kcal/mol, − 6.38 kcal/mol, − 7.59 kcal/mol, − 7.44 kcal/mol and -7.62, respectively (Table 5).

Table 5. SwissDock interaction result of selected hit compounds with CTLA-4 (PDBID: 3OSK)

Compound	**Full fitness (kcal/mol)**	**Gibbs free energy Δ (kcal/mol)**
ZINC85867378	-1083.84	-7.76
ZINC16267039	-1048.60	-6.38
ZINC64219346	-1124.13	-7.59
ZINC68604154	1079.47	-7.44
ZINC20576138	-952.71	-7.62

Fig. 11 SwissDock interaction result of selected hit compounds with CTLA-4 (PDBID: 3OSK)

3.5 Drug likeness property and ADME-tox prediction

The druglikeness property assessment was conducted for the 5 selected molecules (ZINC85867378, ZINC16267039, ZINC64219346, ZINC68604154 and ZINC20576138) with Gibbs free energy < - 9 kcal/mol. (Table 6) ZINC16267039 and ZINC68604154 were predicted to follow the Lipinski's rule of five. Moreover, ZINC68604154 appeared to have better solubility compare to ZINC16267039.

Table 6 The druglikeness properties of five selected molecules from SwissADME

Name	Lipinski's Rule of Five					Drug-Likeness	Water Solubility Class LogS (ESOL)/ LogS (Ali)/ LogS (SILICOS-IT)
	Molecular Weight (g/mol)	Lipophilicity (MLog P)	Hydrogen Bond Donors	Hydrogen Bond Acceptors	No. of Rule Violations	Lipinski's Rule Follows	
	Lee than 500	Less than 4.15	Less than 5	Less than 10	Less than 2 Violations		
ZINC85867378	586.61	-9.55	15	12	3 violations	No	Highly soluble/ Highly soluble/ Soluble
ZINC16267039	460.54	-3.09	1	6	0 violation	Yes	Soluble/ Soluble/ Moderately soluble

ZINC64219346	518.61	0.42	5	6	2 violations	No	Soluble/ Soluble/ Moderately soluble
ZINC68604154	372.50	-7.34	2	6	0 violation	Yes	Highly soluble/ Highly soluble/ Soluble
ZINC20576138	501.88	1.79	9	6	2 violations	No	Moderately soluble/ Poorly soluble// Moderately soluble

The results of the ADMET test for the 5 selected molecules (ZINC85867378, ZINC16267039, ZINC64219346, ZINC68604154 and ZINC20576138) with Gibbs free energy < - 9 kcal/mol are summarized in Table 7. In the absorption section, ZINC16267039 and ZINC20576138 predicted to be optimal Caco-2 permeable. ZINC64219346, ZINC68604154 and ZINC20576138 have better human oral bioavailability than ZINC85867378 and ZINC16267039. Whereas all of them were P-gp (P-glycoprotein) non-inhibitors. ZINC85867378, ZINC16267039 and ZINC64219346 were P-gp substrates. In the distribution section, ZINC20576138 showed high protein binding and low fraction unbound in plasma. ZINC16267039 and ZINC64219346 showed relatively poor performance with no capacity to be blood-brain barrier (BBB) permeable. In the metabolism section, ZINC85867378 and ZINC64219346 were found to be low cytochrome P450 (CYP) mediated drug-drug interaction. ZINC16267039 was predicted to be CYP2C19 substrate and CYP3A4 substrate. ZINC68604154 was CYP2C19 substrate and CYP2D6 substrate. ZINC20576138 was CYP2C19 inhibitor, CYP2C9 inhibitor, CYP2C9 substrate and CYP3A4 inhibitor. In the excretion section, all the compounds were found to have low to medium clearance. In the toxicity section, ZINC16267039 was Ames positive. ZINC64219346 was found to be drug induced liver toxicity (DILI) positive and human hepatotoxicity positive. ZINC20576138 was predicted to be DILI positive, human hepatotoxicity positive, Ames positive and carcinogenicity positive.

Table 7 The ADMET and toxicity properties of five selected molecules from ADMETlab

Class	Properties	ZINC85867378	ZINC16267039	ZINC64219346	ZINC68604154	ZINC20576138
Absorption	Caco-2 permeability	Poor (-6.269 log cm/s)	Proper (-4.902 log cm/s)	Poor (-6.019 log cm/s)	Poor (-5.871 log cm/s)	Proper (-4.654 log cm/s)
	Human oral bioavailability 20% (F20%)	High likelihood F20%<20%	High likelihood F20%<20%	Low likelihood F20%<20%	Low likelihood F20%<20%	Low likelihood F20%<20%
	Pgp-inhibitor	Low likelihood	Low likelihood	Low likelihood	Low likelihood	Low likelihood
	Pgp-substrate	High likelihood	High likelihood	High likelihood	Low likelihood	Low likelihood
Distribution	Plasma Protein Binding (PPB)	11.119%	73.087	33.933%	32.438%	High protein bound (99.946%)
	Volume Distribution (VD)	0.250 L/kg	1.951 L/kg	0.300 L/kg	1.481 L/kg	1.039 L/kg
	Blood-Brain Barrier (BBB)	Medium	Poor	Proper	Medium	Medium
	Fraction unbound in plasms (Fu)	77.197%	35.291%	59.274%	82.464%	Low (1.779%)
Metabolism	CYP1A2 inhibitor	Low likelihood	Low likelihood	Low likelihood	Low likelihood	High likelihood
	CYP 1A2 substrate	Low likelihood	High likelihood	Low likelihood	Low likelihood	Low likelihood
	CYP2C19 inhibitor	Low likelihood	Low likelihood	Low likelihood	Low likelihood	High likelihood

	CYP2C19 substrate	Low likelihood	High likelihood	Low likelihood	High likelihood	Low likelihood
	CYP2C9 inhibitor	Low likelihood	Low likelihood	Low likelihood	Low likelihood	High likelihood
	CYP2C9 substrate	Low likelihood	Low likelihood	Low likelihood	Low likelihood	High likelihood
	CYP2D6 inhibitor	Low likelihood	Low likelihood	Low likelihood	Low likelihood	Low likelihood
	CYP2D6 substrate	Low likelihood	High likelihood	Low likelihood	High likelihood	Low likelihood
	CYP3A4 inhibitor	Low likelihood	Low probability	Low likelihood	Low likelihood	High likelihood
	CYP3A4 substrate	Low likelihood	Low likelihood	Low likelihood	Low likelihood	Low likelihood
Excretion	Clearance (CL)	Low 0.787 mL/min/kg	Low 3.359 mL/min/kg	Moderate 5.239 mL/min/kg	Low 4.481 mL/min/kg	Low 0.73 mL/min/kg
Toxicity	hERG Blockers	Low risk	Low risk	Low risk	Low risk	Low risk
	Human hepatotoxicity	Low risk	Low risk	High risk	Low risk	High risk
	DILI	Low risk	Low risk	High risk	Low risk	High risk
	AMES Toxicity	Low risk	High risk	Low risk	Low risk	High risk
	Carcinogencity	Low risk	Low risk	Low risk	Low risk	High risk

3.6 Network analysis highlights non-random interconnectivity between PD-1 and CTLA-4

Interactions between PD-1 and CTLA-4 with other proteins using STRING database provides the description of various interacting partner. PD-1 and CTLA-4 were input as the "seed" proteins to construct the PPI network (Fig. 12). To identify the most significant interactions and achieve a meaningful size for network analysis, ten additional interactors were allowed in the network. The network enrichment p-value was < 1.01e-06, meaning that this connected network has significantly more interactions than expected at random. Such enrichment also indicates that PD-1 and CTLA-4 are, at least partially, biologically connected.

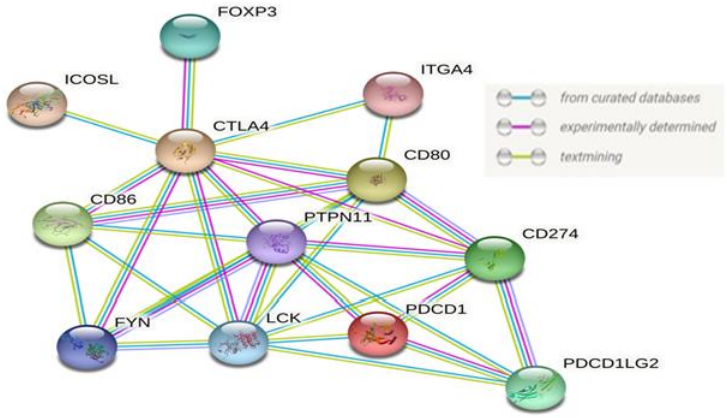

Fig.12: Interaction network resulting between PD-1 and CTLA-4

4. Discussion

The anti-PD-1/PD-L1 check point antibody inhibitors function as tumor suppressors by modulating immune cell-tumor cell interactions and produce notable antitumor effects in cancer immunotherapy.

However, there are some limitations associated with the antibody-based therapies, such as immunogenicity, immune-related adverse events (irAEs), limited modes of administration (intravenous and subcutaneous), low penetration into tissues and high cost. Some of the limitations are difficult to overcome, therefore, it is reasonable to consider discovering orally bioavailable small molecule inhibitors that interrupt the interaction of PD-1 and PD-L1 as alternative [26, 27].

The discovery of new therapeutic drugs is complex, costly, and time-consuming. Leveraging a combination of computational methods can significantly accelerate the drug discovery process, enabling the identification of promising drug candidates from the large compound libraries [35, 36]. Structure-based virtual screening methods offer means to directly identify novel compounds that complement the target protein surface [37, 38]. In order to discover the possible small molecules interacting with the crystal structure of PD-1, we established the workflow combining pharmacophore virtual screening, docking, and ADMET prediction.

In the study, possible ligand binding sites on the PD-1 protein were initially predicted by DoGSiteScorer, FTsite and PrankWeb servers. All the three servers have different algorithms, and their combined results increase probability of where the binding pockets are located in the protein structure. The 6 highest-ranked clusters based on the "druggability" score from PocketQuery were selected as queries for pharmacophore-based virtual screening using ZincPharmer. A total 30 hit compounds identified from ZINCPharmer were retrieved for molecular docking. Among the total 30 compounds, ZINC85867378, ZINC16267039, ZINC64219346, ZINC68604154 and ZINC20576138 are top rank 5 compounds with lowest ΔG values (<-9 kcal/mol), exhibiting possible stronger bindings with PD-1 protein.

The therapeutic success depends on many factors such as physical chemical, pharmacokinetic properties, selectivity, potency, and safety. Various mathematical predictive drug-like properties and pharmacokinetic profiles such as blood-brain-barrier penetration, human intestinal absorption, solubility, cytochrome P450 mediated drug-drug interactions, plasma protein binding was calculated quantitatively for the selected 5 compounds. Thereafter, the selected molecules were subjected to various toxicity screening models such as hepatoxicity cardiac toxicity, AMEs, and carcinogenicity. The meaning of drug-like is dependent on route of administration. The original Lipinski's rule of five deals with orally active compounds and defines four physicochemical parameter ranges: molecular weight (MW) ≤ 500; logP ≤ 5; H-bond donors ≤ 5 and H-bond acceptors ≤ 10[51]. ZINC85867378 presented lowest ΔG values among the selected hit compounds but did not follow the Lipinski's rule of five. Hence, optimization need to further improve the drug-like properties for ZINC85867378. ZINC68604154 appears to have reasonable

oral bioavailability, low DDI potential, and low tox risk. As non P-gp substrate and moderate penetration to brain, ZINC68604154 might also provide some benefit for patients with primary brain tumors or brain metastasis from pharmacokinetics perspective. Moreover, permeability of ZINC68604154 could be further increased by permeation enhancement techniques such as incorporating permeation enhancers into formulations.

Researchers found that combination therapy with the CTLA-4 inhibitor and the PD-1 inhibitor was more effective and resulted in significantly longer progression-free survival compared with monotherapy[52]. As expected, our PPI analysis highlighted non-random interconnectivity between PD-1 and CTLA-4. Interestingly, ZINC85867378, ZINC16267039, ZINC64219346, ZINC68604154 and ZINC20576138 also showed considerable binding affinity with CTLA-4 protein, and potentially dual blockade of PD-1 and CTLA-4.

Despite the abundance of successful cases of drug design relying on computer aided drug design approaches, as with any method, it is not failsafe. Virtual screening and docking can produce potential false positive results, so researchers should be cautious about the limitations of this technique. While the current study was based on in silico predictions, in vitro and in vivo experiments are needed to evaluate whether the identified compounds exhibit strong binding in biological systems. These experiments will further help optimize the drug properties.

5. Conclusion

Cancer is a major burden of disease threatening human health based on its high rates of morbidity and mortality. This study establishes the workflow combining pharmacophore virtual screening, docking, and ADMET prediction to identify the possible small molecules interact with the crystal structure of PD-1. ZINC85867378 presented lowest ΔG value among the selected hit compounds but did not follow the Lipinski's rule of five. ZINC68604154 showed ΔG of -9.07 kcal/mol and appeared to have reasonable oral bioavailability, low DDI potential, and low toxicity risk. The identified compounds might serve as starting points to design potential safe and efficacious molecules in cancer immunotherapy. Further evaluation is necessary to optimize drug properties.

Competing Interests Disclaimer:

Author(s) have declared that they have no known competing financial interests OR non-financial interests OR personal relationships that could have appeared to influence the work reported in this paper.

Ethical Approval

This study used in silico predictions from public databases. Ethical approval is not required.

Disclaimer (Artificial intelligence)

Author(s) hereby declare that NO generative AI technologies such as Large Language Models (ChatGPT, COPILOT, etc.) and text-to-image generators have been used during the writing or editing of this manuscript.

Reference

1. Siegel, R.L., K.D. Miller, and A. Jemal, *Cancer statistics, 2020.* CA Cancer J Clin, 2020. **70**(1): p. 7-30.
2. Sung, H., et al., *Global Cancer Statistics 2020: GLOBOCAN Estimates of Incidence and Mortality Worldwide for 36 Cancers in 185 Countries.* CA Cancer J Clin, 2021. **71**(3): p. 209-249.
3. Wu, W. and S. Zhao, *Metabolic changes in cancer: beyond the Warburg effect.* Acta Biochim Biophys Sin (Shanghai), 2013. **45**(1): p. 18-26.
4. Hanahan, D. and R.A. Weinberg, *Hallmarks of cancer: the next generation.* Cell, 2011. **144**(5): p. 646-74.
5. Pedersen, A.W., et al., *Immunoregulatory antigens-novel targets for cancer immunotherapy.* Chin Clin Oncol, 2018. **7**(2): p. 19.
6. Arruebo, M., et al., *Assessment of the evolution of cancer treatment therapies.* Cancers (Basel), 2011. **3**(3): p. 3279-330.
7. Pardoll, D.M., *The blockade of immune checkpoints in cancer immunotherapy.* Nat Rev Cancer, 2012. **12**(4): p. 252-64.
8. Khalil, D.N., et al., *The future of cancer treatment: immunomodulation, CARs and combination immunotherapy.* Nat Rev Clin Oncol, 2016. **13**(5): p. 273-90.
9. Quezada, S.A. and K.S. Peggs, *Exploiting CTLA-4, PD-1 and PD-L1 to reactivate the host immune response against cancer.* Br J Cancer, 2013. **108**(8): p. 1560-5.
10. Turajlic, S., M. Gore, and J. Larkin, *First report of overall survival for ipilimumab plus nivolumab from the phase III Checkmate 067 study in advanced melanoma.* Ann Oncol, 2018. **29**(3): p. 542-543.
11. Rahimi Kalateh Shah Mohammad, G., et al., *Cytokines as potential combination agents with PD-1/PD-L1 blockade for cancer treatment.* J Cell Physiol, 2020. **235**(7-8): p. 5449-5460.
12. Berman, H.M., et al., *The Protein Data Bank.* Nucleic Acids Res, 2000. **28**(1): p. 235-42.
13. Han, Y., D. Liu, and L. Li, *PD-1/PD-L1 pathway: current researches in cancer.* Am J Cancer Res, 2020. **10**(3): p. 727-742.
14. Ishida, Y., et al., *Induced expression of PD-1, a novel member of the immunoglobulin gene superfamily, upon programmed cell death.* Embo j, 1992. **11**(11): p. 3887-95.

15. Keir, M.E., et al., *PD-1 and its ligands in tolerance and immunity.* Annu Rev Immunol, 2008. **26**: p. 677-704.
16. Fourcade, J., et al., *Upregulation of Tim-3 and PD-1 expression is associated with tumor antigen-specific CD8+ T cell dysfunction in melanoma patients.* J Exp Med, 2010. **207**(10): p. 2175-86.
17. De Sousa Linhares, A., et al., *Therapeutic PD-L1 antibodies are more effective than PD-1 antibodies in blocking PD-1/PD-L1 signaling.* Sci Rep, 2019. **9**(1): p. 11472.
18. Freeman, G.J., et al., *Engagement of the PD-1 immunoinhibitory receptor by a novel B7 family member leads to negative regulation of lymphocyte activation.* J Exp Med, 2000. **192**(7): p. 1027-34.
19. Latchman, Y., et al., *PD-L2 is a second ligand for PD-1 and inhibits T cell activation.* Nat Immunol, 2001. **2**(3): p. 261-8.
20. Carter, L., et al., *PD-1:PD-L inhibitory pathway affects both CD4(+) and CD8(+) T cells and is overcome by IL-2.* Eur J Immunol, 2002. **32**(3): p. 634-43.
21. Sharpe, A.H., et al., *The function of programmed cell death 1 and its ligands in regulating autoimmunity and infection.* Nat Immunol, 2007. **8**(3): p. 239-45.
22. Zitvogel, L. and G. Kroemer, *Targeting PD-1/PD-L1 interactions for cancer immunotherapy.* Oncoimmunology, 2012. **1**(8): p. 1223-1225.
23. Bruehl, F., et al., *State of PD-L1 and PD-1 screening and therapy in NSCLC.* Diagnostic Pathology, 2018. **4**(1).
24. Guo, L., et al., *Clinical and Recent Patents Applications of PD-1/PD-L1 Targeting Immunotherapy in Cancer Treatment-Current Progress, Strategy, and Future Perspective.* Front Immunol, 2020. **11**: p. 1508.
25. Chen, Y., et al., *Looking for the Optimal PD-1/PD-L1 Inhibitor in Cancer Treatment: A Comparison in Basic Structure, Function, and Clinical Practice.* Front Immunol, 2020. **11**: p. 1088.
26. Yang, J. and L. Hu, *Immunomodulators targeting the PD-1/PD-L1 protein-protein interaction: From antibodies to small molecules.* Med Res Rev, 2019. **39**(1): p. 265-301.
27. Zhan, M.M., et al., *From monoclonal antibodies to small molecules: the development of inhibitors targeting the PD-1/PD-L1 pathway.* Drug Discov Today, 2016. **21**(6): p. 1027-36.
28. Ni, L. and C. Dong, *New checkpoints in cancer immunotherapy.* Immunol Rev, 2017. **276**(1): p. 52-65.
29. Lee, J.J., et al., *Phase 1 trial of CA-170, a novel oral small molecule dual inhibitor of immune checkpoints PD-1 and VISTA, in patients (pts) with advanced solid tumor or lymphomas.* Journal of Clinical Oncology, 2017. **35**(15_suppl): p. TPS3099-TPS3099.
30. Musielak, B., et al., *CA-170 - A Potent Small-Molecule PD-L1 Inhibitor or Not?* Molecules, 2019. **24**(15).
31. *33rd Annual Meeting & Pre-Conference Programs of the Society for Immunotherapy of Cancer (SITC 2018): Late-Breaking Abstracts.* Journal for ImmunoTherapy of Cancer, 2018. **6**(2): p. 1-13.
32. Abdel-Magid, A.F., *Inhibitors of the PD-1/PD-L1 Pathway Can Mobilize the Immune System: An Innovative Potential Therapy for Cancer and Chronic Infections.* ACS Med Chem Lett, 2015. **6**(5): p. 489-90.
33. Zak, K.M., et al., *Structural basis for small molecule targeting of the programmed death ligand 1 (PD-L1).* Oncotarget, 2016. **7**(21): p. 30323-35.
34. Han, Y., et al., *Small Molecular Immune Modulators as Anticancer Agents.* Adv Exp Med Biol, 2020. **1248**: p. 547-618.
35. Qing X, L.X., De Raeymaecker J, Tame J, Zhang K, De Maeyer M, Voet A. *A Pharmacophore modeling: advances, limitations, and current utility in drug discovery* Journal of Receptor, Ligand and Channel Research 2014 [cited 7; 81-92]. Available from: https://doi.org/10.2147/JRLCR.S4684.
36. Meng, X.Y., et al., *Molecular docking: a powerful approach for structure-based drug discovery.* Curr Comput Aided Drug Des, 2011. **7**(2): p. 146-57.
37. Crisan, L., S. Avram, and L. Pacureanu, *Pharmacophore-based screening and drug repurposing exemplified on glycogen synthase kinase-3 inhibitors.* Mol Divers, 2017. **21**(2): p. 385-405.

38. Akhtar, N., et al., *Structure-based pharmacophore models to probe anticancer activity of inhibitors of protein kinase B-beta (PKB β).* Chem Biol Drug Des, 2019. **93**(3): p. 325-336.
39. Talevi, A., *Computer-Aided Drug Design: An Overview.* Methods Mol Biol, 2018. **1762**: p. 1-19.
40. Koes, D.R. and C.J. Camacho, *PocketQuery: protein-protein interaction inhibitor starting points from protein-protein interaction structure.* Nucleic Acids Res, 2012. **40**(Web Server issue): p. W387-92.
41. Assis, T.M., et al., *In Silico Study of Leishmania donovani α-β Tubulin and Inhibitors.* Journal of Chemistry, 2014. **2014**: p. 492579.
42. Volkamer, A., et al., *Combining global and local measures for structure-based druggability predictions.* J Chem Inf Model, 2012. **52**(2): p. 360-72.
43. Ngan, C.H., et al., *FTSite: high accuracy detection of ligand binding sites on unbound protein structures.* Bioinformatics, 2012. **28**(2): p. 286-7.
44. Jendele, L., et al., *PrankWeb: a web server for ligand binding site prediction and visualization.* Nucleic Acids Res, 2019. **47**(W1): p. W345-w349.
45. Krivák, R. and D. Hoksza, *P2Rank: machine learning based tool for rapid and accurate prediction of ligand binding sites from protein structure.* J Cheminform, 2018. **10**(1): p. 39.
46. Shin, W.H., C.W. Christoffer, and D. Kihara, *In silico structure-based approaches to discover protein-protein interaction-targeting drugs.* Methods, 2017. **131**: p. 22-32.
47. Grosdidier, A., V. Zoete, and O. Michielin, *SwissDock, a protein-small molecule docking web service based on EADock DSS.* Nucleic Acids Res, 2011. **39**(Web Server issue): p. W270-7.
48. Daina, A., O. Michielin, and V. Zoete, *SwissADME: a free web tool to evaluate pharmacokinetics, drug-likeness and medicinal chemistry friendliness of small molecules.* Scientific Reports, 2017. **7**(1): p. 42717.
49. Dong, J., et al., *ADMETlab: a platform for systematic ADMET evaluation based on a comprehensively collected ADMET database.* J Cheminform, 2018. **10**(1): p. 29.
50. Szklarczyk, D., et al., *STRING v11: protein-protein association networks with increased coverage, supporting functional discovery in genome-wide experimental datasets.* Nucleic Acids Res, 2019. **47**(D1): p. D607-d613.
51. Lipinski, C.A., et al., *Experimental and computational approaches to estimate solubility and permeability in drug discovery and development settings.* Adv Drug Deliv Rev, 2001. **46**(1-3): p. 3-26.
52. Larkin, J., et al., *Five-Year Survival with Combined Nivolumab and Ipilimumab in Advanced Melanoma.* N Engl J Med, 2019. **381**(16): p. 1535-1546.